

RESEARCH NOTE

# Viscoelastic perturbations of the earth: significance of the incremental gravitational force in models of glacial isostasy

Falk Amelung\* and Detlef Wolf

Institute of Planetology, University of Münster, Wilhelm-Klemm-Straße 10, D-48149 Münster, Germany

Accepted 1993 November 12. Received 1993 October 28; in original form 1992 September 29

## SUMMARY

The *incremental gravitational force* (IGF) arises from perturbations of the earth's gravitational potential. In glacial isostasy, its sources are the *surficial* and *internal mass redistributions* associated with the growth and decay of the continental ice sheets.

We examine the errors caused by the neglect of the IGF using closed-form solutions of the equations governing surface-load induced perturbations of two types of incompressible, spherical-earth models: (1) *Maxwellian-viscoelastic* mantle enclosed by *elastic* lithosphere, and (2) *Maxwellian-viscoelastic* mantle enclosing *inviscid* core. Calculations in the Legendre domain of the radial surface displacement for these models show that neglecting the IGF causes enhancement of the elastic response and acceleration of the viscous relaxation. In the space domain, these changes entail corresponding modifications of the calculated land adjustment. The magnitude of the error caused by the neglect of the IGF strongly depends on the deglaciation history and load radius adopted. Assuming a typical deglaciation history, the error reaches a maximum of less than 20 m at the end of the deglaciation phase for loads comparable in size to the Canadian or the Fennoscandian ice sheets.

We also compare *spherical-earth* models with IGF and *plane-earth* models without IGF. Calculations of the radial surface displacement show that the errors due to the neglect of sphericity and the IGF partially compensate each other. Taking the uncertainties of the observational data into account, we conclude that the majority of the Canadian and Fennoscandian glacial-isostatic adjustment data can be modelled with sufficient accuracy using a plane-earth model without IGF.

**Key words:** glacial-isostatic adjustment, gravitational viscoelastodynamics, incremental gravitational force, Maxwellian viscoelasticity, plane-earth approximation.

## 1 INTRODUCTION

The uplift of the formerly ice-covered areas in Canada and Fennoscandia since the end of the Pleistocene and the simultaneous subsidence of the peripheral regions are one of the main sources of information on the viscosity of the earth's mantle and the thickness of its elastic lithosphere. Our knowledge of the values of these parameters is based on comparisons between several types of observation of

glacial-isostatic adjustment and calculations based on simplified earth and load models. Thus, the Canadian data have commonly been modelled using spherical-earth models with Maxwellian-viscoelastic rheology (e.g. Cathles 1975, pp. 196–255; Wu & Peltier 1983; Wolf 1985; Mitrovica & Peltier 1989); for the Fennoscandian data, plane-earth models with the same rheology have usually been employed (e.g. Cathles 1975, pp. 173–196; Wolf 1987; Fjeldskaar & Cathles 1991).

In several recent studies, a number of special features of the earth's interior have been examined more closely. These features include (1) continuous increase of density with

\* Present address: EOPG, 5 Rue René Descartes, F-67084 Strasbourg, France.

depth due to self-compression (e.g. Wu & Yuen 1991), (2) lateral heterogeneities of viscosity and lithosphere thickness due to temperature variations (e.g. Gasperini & Sabadini 1989), and (3) generalized viscoelastic rheologies (e.g. K ornig & M uller 1989; Wu 1992). A common characteristic of these studies is that, for simplicity, the gravitational force is taken as unperturbed: the *incremental-gravitational-force* (IGF) term in the equilibrium equation is neglected. Such earth models have sometimes been referred to as externally gravitating; earth models with the IGF included are commonly known as self-gravitating. In general, the neglect of the IGF has been justified by arguing that, compared to the mass of the earth, the masses of even the major glacial loads are sufficiently small that the gravitational effects associated with them can be ignored. The principal objective of the present study is to examine the validity of this argument in detail.

A related question is whether the use of *plane-earth models*, an approximation adopted in several of the studies mentioned above, affects the results of interpretations significantly. This problem was addressed by Wolf (1984), who concluded that sphericity can be neglected in studies of the ‘regional’ Fennoscandian glacial-isostatic adjustment process, but not necessarily in studies of the ‘global’ Canadian process. However, Wolf compared plane-earth models without IGF with spherical-earth models without IGF. We show, by comparison with spherical-earth models with IGF, that Wolf’s results must be modified: in fact, most of the Canadian readjustment data can be modelled with an accuracy similar to that achieved for the Fennoscandian data by using plane-earth models without IGF.

In the following section, we will state the equations governing quasi-static gravitational-viscoelastic perturbations, induced by interface loading, of an incompressible, non-rotating and initially hydrostatic fluid earth (Section 2). Using *closed-form* solutions to the equations governing models with or without IGF, we will then compare the calculated values of several observables of postglacial adjustment (Section 3). Emphasis will be laid on the radial surface displacement and the error incurred in its calculation due to the neglect of the IGF; furthermore, the dependence of the IGF on the size of the ice sheet and the history of the deglaciation adopted in the model will be investigated. Our study concludes with a brief summary of the results obtained (Section 4).

## 2 FIELD EQUATIONS AND INTERFACE CONDITIONS: TENSOR FORMS

We compile the field equations and interface conditions for the initial fields (Section 2.1) and the incremental fields (Section 2.2) governing perturbations of an initially hydrostatic fluid. For this, we use Cartesian tensor fields in indicial notation with the usual summation and differentiation conventions and employ the *Lagrangian* kinematic formulation. In particular, we take  $t = 0$  as *initial* time,  $t \in [0, \infty)$  as *current* time, and the initial particle position,  $X_i \in \mathcal{X} \cup \partial\mathcal{X}$ , as spatial argument, with  $\mathcal{X}$  the domain occupied by the fluid in the initial state and  $\partial\mathcal{X}$  the interfaces of discontinuity of particular parameters of the fluid in that state. We also assume that, for all  $X_i \in \mathcal{X}$ , the current value of an arbitrary field,  $f_{ij\dots}(\mathbf{X}, t)$ , can be

described as infinitesimal perturbation of its initial value,  $f_{ij\dots}^{(0)}(\mathbf{X})$ , and expressed alternatively in terms of the *material incremental field*,  $f_{ij\dots}^{(\delta)}(\mathbf{X}, t)$ , referring to the particle initially at position  $X_i$ , or in terms of the *local incremental field*,  $f_{ij\dots}^{(\Delta)}(\mathbf{X}, t)$ , referring to the position  $X_i$ . For  $X_i \in \partial\mathcal{X}$ , the fields satisfy certain interface conditions. They are stated concisely using the definition  $[f_{ij\dots}(\mathbf{X}, t)]_{\pm}^{\pm} = \lim_{\Delta\mathbf{X} \rightarrow 0} f_{ij\dots}(\mathbf{X} + \Delta\mathbf{X}, t) - \lim_{\Delta\mathbf{X} \rightarrow 0} f_{ij\dots}(\mathbf{X} - \Delta\mathbf{X}, t)$ . In the following, we will usually suppress the spatial and temporal arguments. More detailed accounts on the formulations of the field equations and interface conditions can be found elsewhere (e.g. Wolf 1991a, 1994).

### 2.1 Initial state

Suppose that the fluid is incompressible, non-rotating and free from non-gravitational volume forces and that the interfaces are initially unforced. Then, the field equations and interface conditions governing a hydrostatic initial state are

$$\left. \begin{aligned} p_{,i}^{(0)} - \rho\phi_{,i}^{(0)} &= 0 \\ \phi_{,ii}^{(0)} &= -4\pi G\rho \end{aligned} \right\} X_i \in \mathcal{X}, \quad (1)$$

$$\left. \begin{aligned} [p^{(0)}]_{\pm}^{\pm} &= 0 \\ [\phi^{(0)}]_{\pm}^{\pm} &= 0 \end{aligned} \right\} X_i \in \partial\mathcal{X}, \quad (3)$$

$$[\phi_{,i}^{(0)}]_{\pm}^{\pm} = 0 \quad (4)$$

$$[\phi_{,i}^{(0)}]_{\pm}^{\pm} = 0 \quad (5)$$

where  $p^{(0)}$  is the initial mechanical pressure,  $\phi^{(0)}$  the initial gravitational potential,  $\rho$  the volume-mass density and  $G$  Newton’s gravitational constant. Eqs (1) and (2) are referred to as initial equilibrium equation and initial potential equation. With  $\rho$  prescribed, (1) and (2) constitute a system of linear partial differential equations for  $p^{(0)}$  and  $\phi^{(0)}$ , whose solution must satisfy (3)–(5).

### 2.2 Incremental state

Assume that the fluid undergoes quasi-static gravitational-viscoelastic perturbations in response to incremental masses located on the interfaces. With  $\tilde{f}_{ij\dots}(\mathbf{X}, s)$  denoting the Laplace transform of  $f_{ij\dots}(\mathbf{X}, t)$  with respect to  $t$  (e.g. LePage 1980, pp. 285–318), the following Laplace-transformed incremental-field equations and interface conditions apply:

$$\tilde{u}_{i,i} = 0 \quad (6)$$

$$\left. \begin{aligned} \tilde{t}_{ij,j}^{(\delta)} + (\rho\phi_{,j}^{(0)}\tilde{u}_j)_{,i} + \rho\tilde{\phi}_{,i}^{(\Delta)} &= 0 \\ \tilde{t}_{ij}^{(\delta)} &= -\tilde{p}^{(\delta)}\delta_{ij} + s\tilde{m}(\tilde{u}_{i,j} + \tilde{u}_{j,i}) \end{aligned} \right\} X_i \in \mathcal{X}, \quad (7)$$

$$\tilde{\phi}_{,ii}^{(\Delta)} = 0 \quad (8)$$

$$[\tilde{u}_i]_{\pm}^{\pm} = 0 \quad (9)$$

$$\left. \begin{aligned} [n_i^{(0)}\tilde{t}_{ij}^{(\delta)}]_{\pm}^{\pm} &= -\phi_{,i}^{(0)}\tilde{\sigma} \\ [\tilde{\phi}^{(\Delta)}]_{\pm}^{\pm} &= 0 \end{aligned} \right\} X_i \in \partial\mathcal{X}. \quad (10)$$

$$[n_i^{(0)}(\tilde{\phi}_{,i}^{(\Delta)} - 4\pi G\rho\tilde{u}_i)]_{\pm}^{\pm} = -4\pi G\tilde{\sigma} \quad (11)$$

Referring to Laplace-transformed incremental fields simply as incremental fields,  $\tilde{m}$  is the shear relaxation function,  $\tilde{p}^{(\delta)}$  the material incremental mechanical pressure,  $\tilde{t}_{ij}^{(\delta)}$  the material incremental Cauchy stress,  $\tilde{u}_i$  the displacement,  $\tilde{\phi}^{(\Delta)}$  the local incremental gravitational potential and  $\tilde{\sigma}$  the incremental interface-mass density. We have also used  $n_i^{(0)}$ ,

which is the unit normal with respect to  $\partial\mathcal{X}$  and anti-parallel to  $\phi_i^{(0)}$ ; note that  $n_i^{(0)}$  is directed to the positive side of  $\partial\mathcal{X}$ . Eqs (6)–(9) are referred to as incremental incompressibility condition, incremental equilibrium equation, incremental constitutive equation of viscoelasticity and incremental potential equation. With  $\bar{m}$ ,  $\rho$  and  $\bar{\sigma}$  taken as prescribed and  $\phi^{(0)}$  given as special solution to (1)–(5), eqs (6)–(9) constitute a system of linear partial differential equations for  $\bar{p}^{(\delta)}$ ,  $\bar{i}_{ij}^{(\delta)}$ ,  $\bar{u}_i$  and  $\bar{\phi}^{(\Delta)}$ , whose solution must satisfy (10)–(13).

The term  $\rho\bar{\phi}_i^{(\Delta)}$  in (7) is the *incremental gravitational force* (IGF) per unit mass. Obviously, it couples the *mechanical* quantities,  $\bar{p}^{(\delta)}$ ,  $\bar{i}_{ij}^{(\delta)}$  and  $\bar{u}_i$ , with the *gravitational* quantity,  $\bar{\phi}^{(\Delta)}$ . Earth models governed by (6)–(9) are commonly referred to as self-gravitating. Frequently, the gravitational force is taken as unperturbed, i.e. the IGF is neglected. Then, the mechanical quantities decouple from the gravitational quantity. The corresponding earth model has sometimes been referred to as externally gravitating. However, even in this case, the initial state is usually taken as self-gravitating and governed by (1) and (2). In the following, we will avoid the terms self-gravitating and externally gravitating and, instead, refer to models with IGF and without IGF.

Closed-form solutions to (1)–(13) were given by Wu & Peltier (1982) and Wolf (1994) for a homogeneous sphere and by Wolf (1984) for a two-layer sphere; the IGF was included only in the solutions for the homogeneous sphere. The computational results of the present study are based on closed-form solutions, with or without IGF term in the equilibrium equation, for two spherical-earth models: (1) *Maxwellian-viscoelastic* mantle enclosed by *elastic* lithosphere (earth model *L*) and (2) *Maxwellian-viscoelastic* mantle enclosing *inviscid* core (earth model *C*). The solution for a homogeneous Maxwellian-viscoelastic earth (earth model *H*) follows from either solution as a special case. The corresponding earth models without IGF are distinguished by the primed symbols *L'*, *C'* and *H'*. The integration of the scalar equations and determination of the integration constants is outlined in Appendices A–C.

### 3 COMPUTATIONAL RESULTS

To illustrate the significance of the IGF, we begin with a comparison, in the spherical-harmonic domain, between the radial surface displacement for spherical-earth models with or without IGF (Section 3.1). After that, we will present calculations in the spatial domain and compare radial surface displacement and geoid height for these earth models (Section 3.2). In particular, we will give the numerical values of the errors due to the neglect of the IGF when modelling the Fennoscandian and Canadian glacial-isostatic adjustment processes. Further, we will test the adequacy of the frequently used plane-earth model without IGF by comparing its response with the responses of the corresponding spherical-earth models with or without IGF. The parameters of earth models *H*, *L* and *C* are specified in Table 1. We employ as the viscous parameter the shear viscosity,  $\eta$ , which is related to the inverse Maxwell time,  $\beta$ , and the shear modulus,  $\mu$ , by  $\eta = \mu/\beta$  (Appendix C).

**Table 1.** Parameters of spherical-earth models; symbols *H'*, *L'* and *C'* are used to distinguish models without IGF.

	Earth model H	Earth model L	Earth model C
Radius	$a_2=6371$ km	$a_1=6271$ km $a_2=6371$ km	$a_1=3485$ km $a_2=6371$ km
Density	$\rho_2=5514$ kg m <sup>-3</sup>	$\rho_1=5514$ kg m <sup>-3</sup> $\rho_2=5514$ kg m <sup>-3</sup>	$\rho_1=10630$ kg m <sup>-3</sup> $\rho_2=4510$ kg m <sup>-3</sup>
Shear modulus	$\mu_2=1.45 \times 10^{11}$ Pa	$\mu_1=1.45 \times 10^{11}$ Pa $\mu_2=0.67 \times 10^{11}$ Pa	$\mu_1=0$ $\mu_2=1.45 \times 10^{11}$ Pa
Viscosity	$\eta_2=1 \times 10^{21}$ Pa s	$\eta_1=1 \times 10^{21}$ Pa s $\eta_2=\infty$	$\eta_1=0$ $\eta_2=1 \times 10^{21}$ Pa s

#### 3.1 Spherical-harmonic domain

The spherical-harmonic coefficient of the radial surface displacement for *Heaviside* loading,  $S = S'H(t)$ , is obtained by convolution with the corresponding spherical-harmonic coefficient for *impulse* loading,  $S = S'\delta(t)$  (Appendix D). We get

$$U(a_2, t) = - \left[ T^{(e)} + \sum_{m=1}^M T_m^{(v)} (1 - e^{-s_m t}) \right] \frac{S'}{\rho_2}, \quad (14)$$

where  $M$  is the total number of modes with  $M = 1$  (earth model *H*) or  $M = 2$  (earth models *L* and *C*),  $T^{(e)}$  the elastic amplitude,  $T_m^{(v)}$  the viscous amplitude and  $s_m$  the inverse relaxation time (e.g. Wu & Peltier 1982; Wolf 1984, 1994). The response for  $t \rightarrow \infty$  follows as

$$U(a_2, \infty) = - \left( T^{(e)} + \sum_{m=1}^M T_m^{(v)} \right) \frac{S'}{\rho_2}, \quad (15)$$

where the expression in brackets is called total amplitude,  $T^{(t)}$ . Instead of  $s_m$ , its inverse,  $s_m^{-1}$ , will henceforth be used.

##### 3.1.1 Earth model *H*

Figure 1 shows the elastic, viscous and total amplitudes,  $T^{(e)}$ ,  $T_1^{(v)}$  and  $T^{(t)}$ , and the relaxation time,  $s_1^{-1}$ , as functions of the spherical-harmonic degree,  $n$ , for earth model *H*. The numerical values of the parameters (Table 1) correspond to those of an average earth. The main response characteristics are as follows (e.g. Peltier 1976; Wu & Peltier 1982; Wolf 1984): Whereas  $T^{(e)}$  shows a quasi-linear decrease with increasing  $n$ ,  $T^{(t)}$  corresponds to hydrostatic equilibrium and is therefore independent of  $n$  (Fig. 1a). The transition between  $T^{(e)}$  and  $T^{(t)}$  is carried by a single mode,  $M0$ , which is associated with the density discontinuity at the earth's surface. Its amplitude,  $T_1^{(v)}$ , describes the viscous portion of  $T^{(t)}$  and increases with increasing  $n$  according to the decrease of  $T^{(e)}$  (Fig. 1b). Similarly,  $s_1^{-1}$  increases with increasing values of  $n$  (Fig. 1c).

If the IGF is neglected,  $T^{(e)}$  increases and, since  $T^{(t)}$  is unaffected,  $T_1^{(v)}$  decreases by the same amount, whereas  $s_1^{-1}$  is shortened. As a consequence, the radial surface displacement is enhanced and the final state of hydrostatic equilibrium approached faster. This behaviour applies in particular at small values of  $n$ . It can be explained by noting that the interaction between the masses of earth, load and surface depression decompose into (1) the gravitational

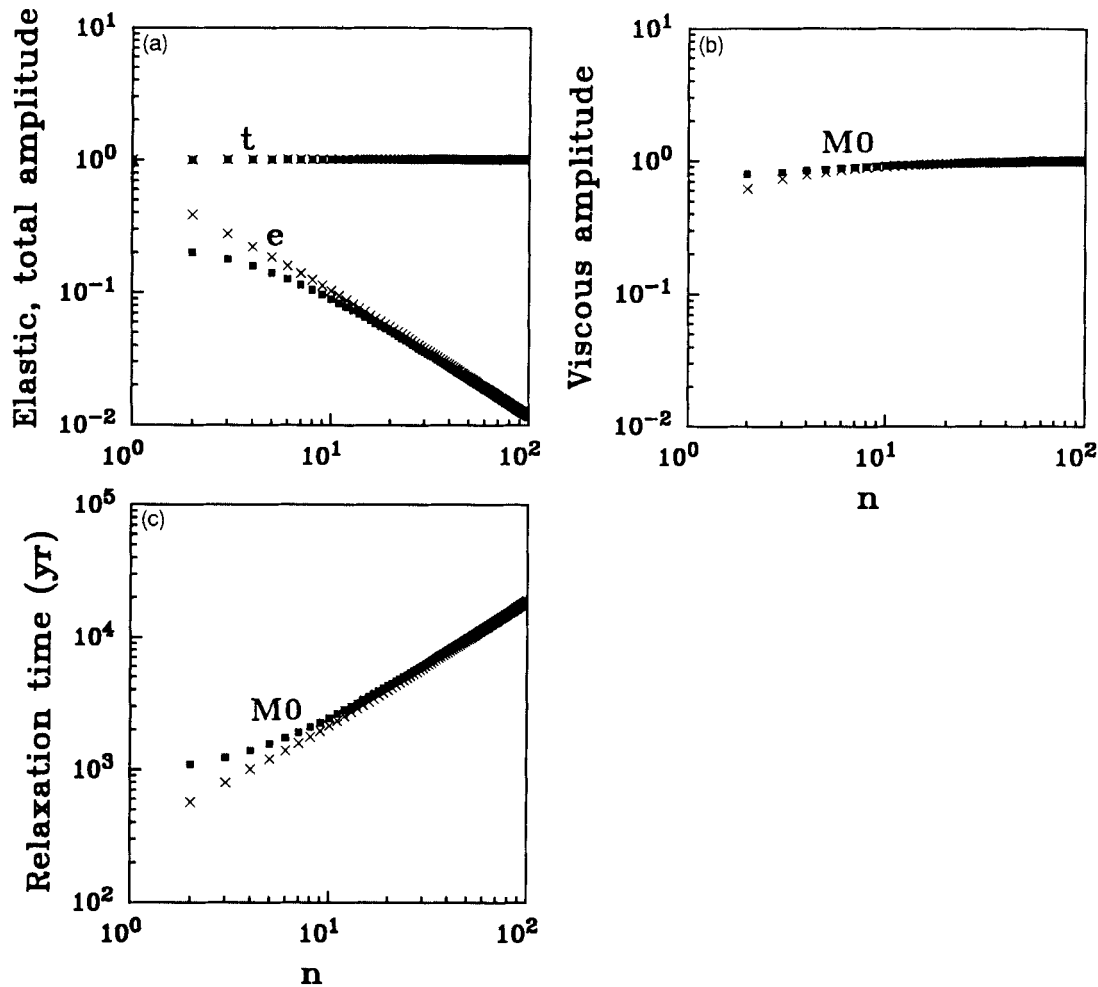


**Figure 1.** (a) Elastic amplitude,  $T^{(e)}$ , and total amplitude,  $T^{(t)}$ , (b) viscous amplitude,  $T^{(v)}$ , and (c) relaxation time,  $1/s_1$ , as functions of spherical-harmonic degree,  $n$ , for earth models  $H$  (squares) and  $H'$  (crosses).  $M0$  denotes relaxation mode.

effect of the earth on the net mass of load and surface depression and (2) the net gravitational effect of load and surface depression on the mass of the earth. Considering that the effects are additive, it is obvious that the radial surface displacement becomes larger in magnitude if the second force, the IGF, is neglected (*cf.* Cathles 1975, p. 80).

### 3.1.2 Earth model L

Earth model  $L$  differs from earth model  $H$  by the inclusion of an elastic lithosphere of 100 km thickness; the shear modulus of the lithosphere (Table 1) corresponds to average values near 100 km depth (Bullen 1975, p. 254). The significance of the lithosphere to glacial isostasy was discussed before (e.g. Wu & Peltier 1982; Wolf 1984); here, the main response characteristics are briefly recalled.

Figure 2 shows that  $T^{(e)}$  and  $T^{(t)}$  differ from those for earth model  $H$  at high values of  $n$ : whereas  $T^{(e)}$  is enhanced slightly,  $T^{(t)}$  no longer corresponds to the amplitude for hydrostatic equilibrium (Fig. 2a). The first effect is due to the reduced shear modulus in the lithosphere; the second arises because the shear energy remains partly stored in the lithosphere. The relaxation is now characterized by two

modes (Fig. 2c). As for earth model  $H$ , the  $M0$  mode is associated with the density discontinuity at the earth's surface, whereas the  $L0$  mode is supported by the viscosity discontinuity at the lithosphere–mantle boundary. However, the total relaxation is mainly carried by the  $M0$  mode. For small values of  $n$ , its amplitude is close to that of the  $M0$  mode in earth model  $H$ . The  $L0$  mode contributes to the relaxation significantly only for  $n = 8$ . In view of the predominantly elastic response of earth model  $L$  for loads of short wavelength, the viscous amplitudes approach 0 for high values of  $n$ . For small  $n$ , the relaxation time associated with the  $M0$  mode approaches that of this mode in earth model  $H$ . However, for large  $n$ , it deviates considerably and approaches the relaxation time for the  $L0$  mode (Fig. 2d).

If the IGF is neglected,  $T^{(e)}$  increases as for earth model  $H$ . The energy partition between the two modes changes but the decrease of their sum (Fig. 2b) resembles the decrease of  $T^{(v)}$  for earth model  $H$ . Also, the shortening of the relaxation time for the  $M0$  mode caused by the neglect of the IGF corresponds to the behaviour of the relaxation time for this mode in earth model  $H$ . On the other hand, due to the presence of the lithosphere, the IGF now no longer vanishes for  $t \rightarrow \infty$  and  $T^{(t)}$  is slightly enhanced if the IGF is

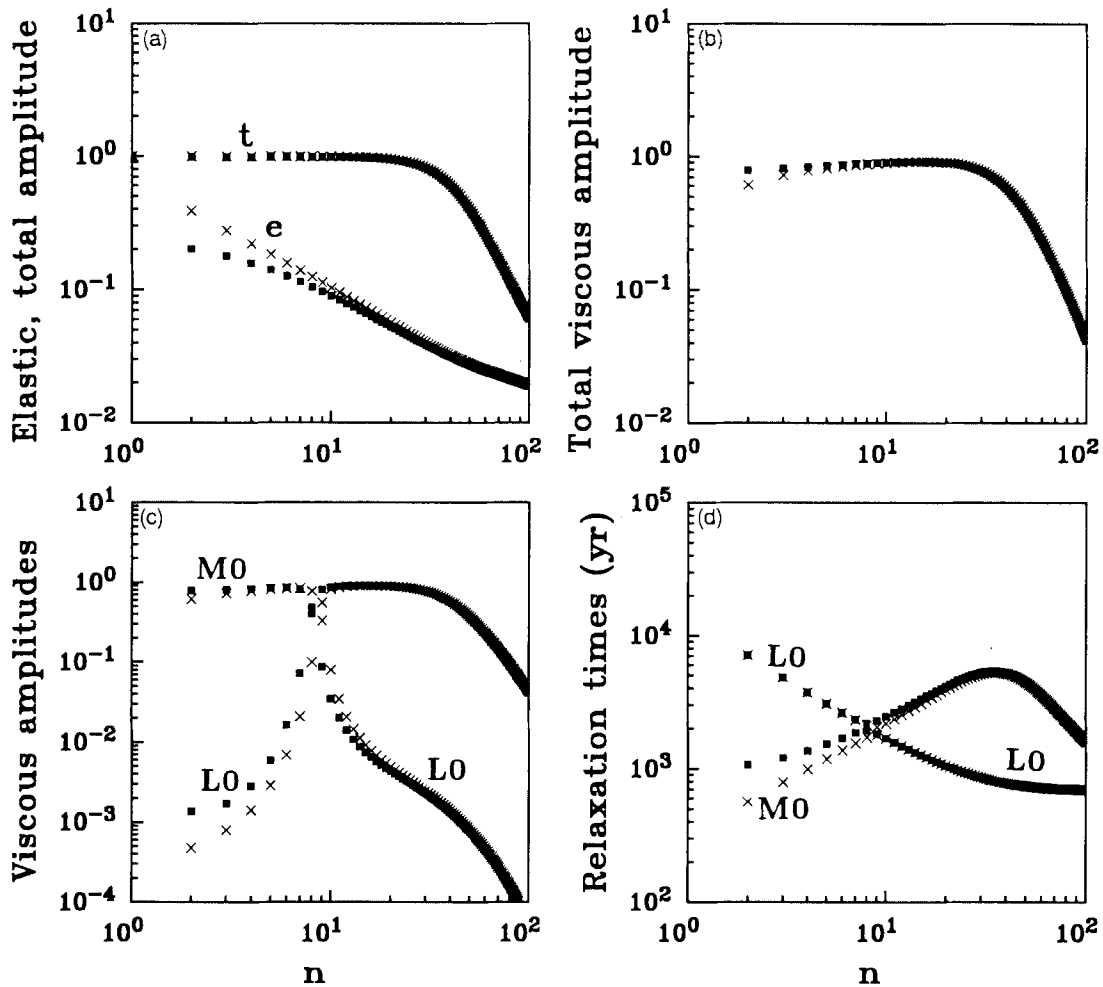


**Figure 2.** (a) Elastic amplitude,  $T^{(e)}$ , and total amplitude,  $T^{(t)}$ , (b) total viscous amplitude,  $T_1^{(v)} + T_2^{(v)}$ , (c) viscous amplitudes,  $T_1^{(v)}$  and  $T_2^{(v)}$ , and (d) relaxation times,  $1/s_1$  and  $1/s_2$ , as functions of spherical-harmonic degree,  $n$ , for earth models  $L$  (squares) and  $L'$  (crosses).  $M_0$  and  $L_0$  denote relaxation modes.

neglected. The latter effect is, however, trifling and cannot be detected on the scale of the figure.

### 3.1.3 Earth model C

Earth model  $C$  is distinguished from earth model  $H$  by the inclusion of an inviscid core. The densities adopted for the core and the mantle (Table 1) ensure correct gravity values at the core–mantle boundary (CMB) and at the earth’s surface:  $\gamma_1 = 10.36 \text{ m s}^{-2}$  and  $\gamma_2 = 9.82 \text{ m s}^{-2}$ , respectively.

In Fig. 3, the response characteristics of earth model  $C$  are illustrated (e.g. Peltier 1976; Wu & Peltier 1982; Wu 1990). Again, the behaviour of  $T^{(e)}$  is similar to that for earth model  $H$ , the deviation for small values of  $n$  being due to the presence of the core. Also,  $T^{(t)}$  is independent of  $n$  and corresponds to that for hydrostatic equilibrium (Fig. 3a). In addition to the  $M_0$  mode, the  $C_0$  mode associated with the density discontinuity at the CMB now appears (Fig. 3c). However, for  $n > 10$  the deformation of the CMB is insignificant and the  $C_0$  mode barely excited. For small values of  $n$ , the relaxation time for the  $C_0$  mode is significantly longer than that for the  $M_0$  mode (Fig. 3d).

If the IGF is neglected, the modifications of the response

are similar to those for earth model  $H$ . Hence, the elastic amplitude increases, the total viscous amplitude decreases, with the energy partition between the  $M_0$  and  $C_0$  modes changing, and the relaxation times are shortened. This suggests that the effects, on the radial surface displacement, due to the IGF arising from the deformation of the CMB are fairly small.

### 3.2 Spatial domain

The objective of this section is to obtain quantitative measures of the errors incurred due to the neglect of the IGF in calculations of the main geophysical observables related to postglacial adjustment: radial surface displacement and geoid height. A principal difficulty in modelling glacial-isostatic adjustment is that the cross-sections and deglaciation histories of the Pleistocene ice sheets are incompletely known. This fact renders any load model to be employed poorly constrained. Since, in this study, no data will be interpreted, it is sufficient to use two fairly elementary load models.

In load model  $A$ , we consider axisymmetric loads with cross-sections corresponding to the spherical harmonics  $Y_n^0$

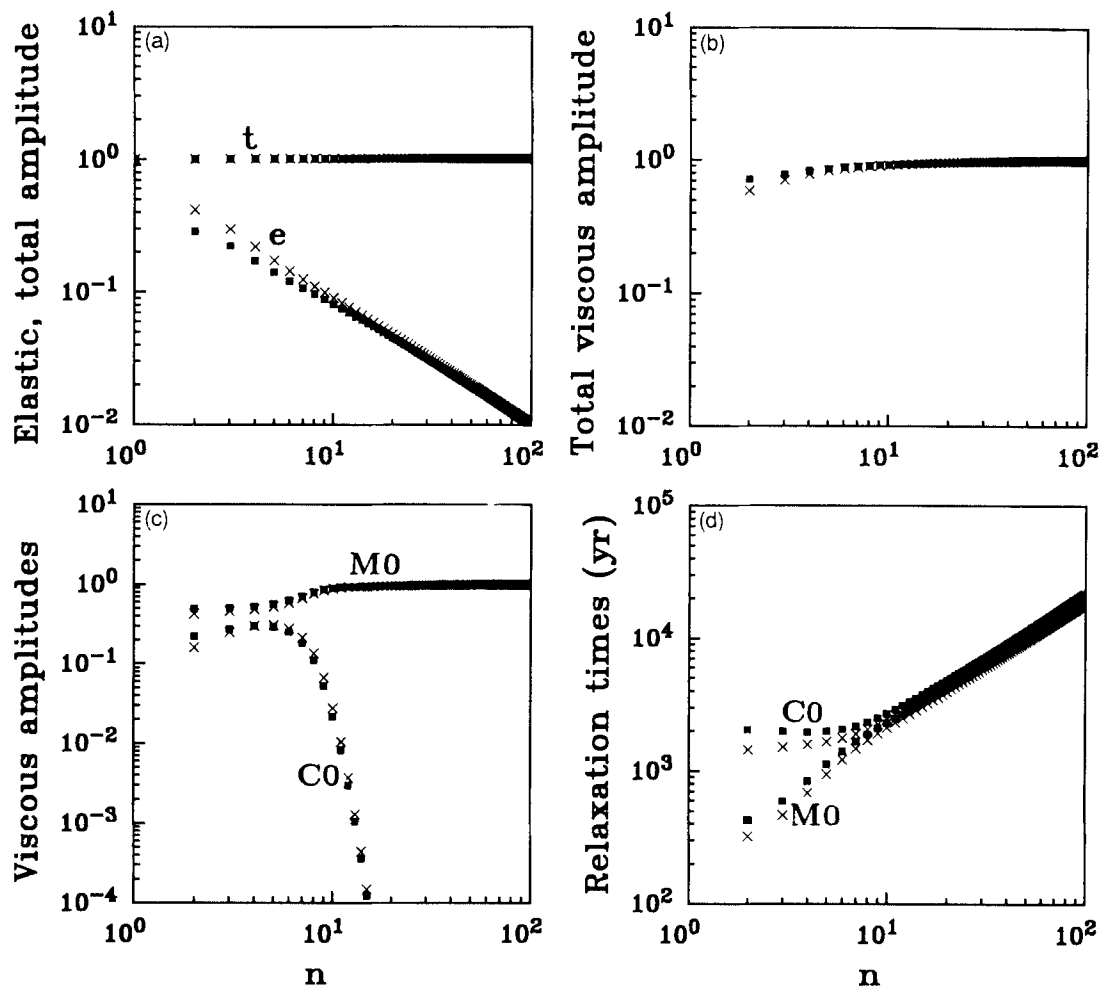


Figure 3. Same as Fig. 2 but for earth models *C* and *C'*. *M0* and *C0* denote relaxation modes.

and  $Y_{1,5}^0$ . If applied to the earth, the intervals inside the first roots of these functions will be comparable to the radii of the Pleistocene Canadian and Fennoscandian ice sheets, respectively. The deglaciation histories are modelled as *instantaneous* unloading at  $t=0$ . For obvious reasons, it is sufficient to calculate field values on the load axes. In load model *B*, we simulate the Canadian and Fennoscandian ice sheets using an axisymmetric disk load with rectangular cross-section and fixed radius of  $R_L=1600$  km and  $R_L=800$  km, respectively. The associated deglaciation histories start at  $t=0$ , are *linear* and finish at  $t=10$  Kyr. Both load models imply that, prior to deglaciation, the earth has been in equilibrium with the load. Computationally, the loading histories are accounted for by convolving them with the impulse response. The calculation of the response to disk loads requires the evaluation of the appropriate spherical-harmonic expansions. All results apply to a load density of  $1000 \text{ kg m}^{-3}$  and a maximum load thickness of 3 km.

### 3.2.1 Load model *A*

In Canada, the postglacial land uplift in the *central* region of the former ice sheet is barely influenced by the lithosphere

but significantly by the core (e.g. Wu & Peltier 1982). On the other hand, the central land uplift in Fennoscandia is moderately sensitive to the presence of the lithosphere (e.g. Wolf 1984) whereas the core is of subordinate importance. This suggests the employment of earth model *C* for modelling the central uplift in Canada and earth model *L* for modelling it in Fennoscandia.

We note that the densities of lithosphere and mantle in earth models *L* and *C*, respectively, are higher than the densities of the earth's upper layers. Since the radial surface displacement in hydrostatic equilibrium is inversely proportional to the upper layer density, the calculated displacements are therefore too small in magnitude. As is shown elsewhere (Amelung 1991), this deficiency of earth models *L* and *C* does not invalidate our conclusions on the significance of the IGF for the interpretation of glacial-isostatic adjustment data.

In Fig. 4, the computational results for earth models *C* and *C'* and load model *A* with  $n=6$  (Canadian ice sheet) are displayed. Fig. 4(a) shows that, in accordance with our expectations, the radial surface displacement becomes smaller in magnitude if the IGF is neglected. The error due to this neglect is shown more clearly in Fig. 4(b). Immediately after load removal, it amounts to 15 m; at

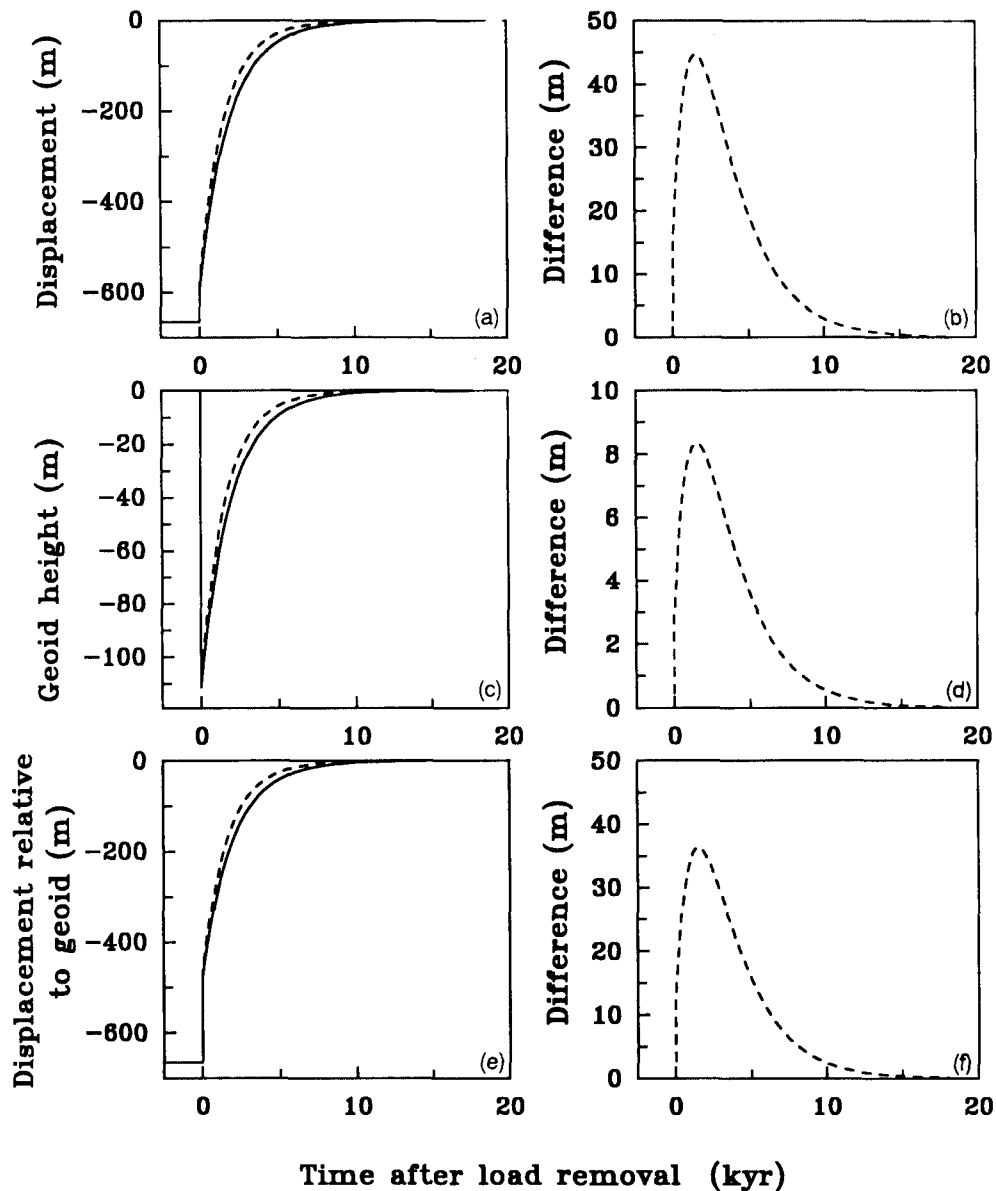


**Figure 4.** (a) Radial surface displacement,  $u_r$ , as a function of time,  $t$ , after load removal for earth models  $C$  (solid) and  $C'$  (dashed) and (b) difference between radial surface displacements for earth models  $C'$  and  $C$ . (c, d) Same as (a) and (b) but for geoid height,  $h$ . (e, f) Same as (a) and (b) but for radial surface displacement relative to geoid,  $u_r - h$ . Calculations apply to axis of load model  $A$  with  $n = 6$ .

about 1.5 Kyr (approximately the relaxation time of the  $M0$  mode for  $n = 6$ ), it has reached its maximum of 45 m; for longer times after unloading, the error decreases and has almost vanished after 10 Kyr. In Figs 4(c) and (d), the corresponding results are given for the geoid height. Because of the mass deficit after unloading, the geoid height is always negative. The time dependences are similar to those for the radial surface displacement. This shows that the deformation of the CMB, which is largely controlled by the relaxation of the  $C0$  mode, affects the geoid height only insignificantly.

We may reasonably assume that the deglaciation of Canada took place 10 Kyr BP such that the time  $t = 10$  Kyr corresponds to the present time. Then, Fig. 4 suggests that hydrostatic equilibrium has been essentially restored in that

region today, and the calculated displacement at a particular time  $t < 10$  Kyr can be interpreted as (the negative of) the land uplift that has occurred since that time. In the first approximation, this uplift is recorded as the elevation of ancient shorelines; as Figs 4(a) and (b) show, the shoreline elevation is underestimated in our calculations if the IGF is neglected. A better approximation is attained if calculations of the radial surface displacement are referred to the geoid. This is because shoreline elevations are taken with respect to the present-day sea surface which, in general, is different from the sea surface at the time of formation of the shoreline. The radial surface displacement relative to the geoid is shown in Fig. 4(e). Since displacement and geoid height are negative, the magnitude of the displacement is reduced if it is referred to the geoid. Likewise, the

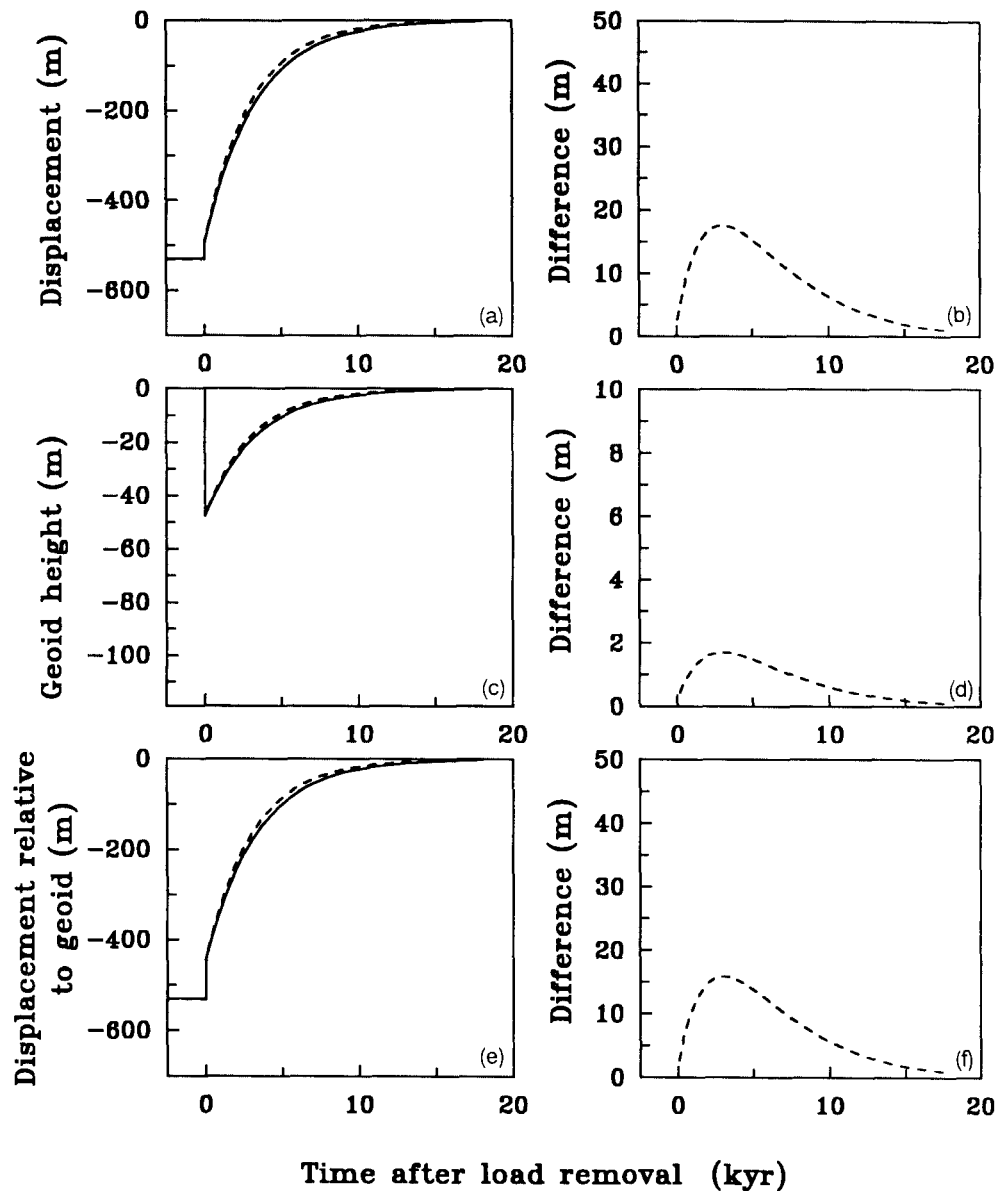


Figure 5. Same as Fig. 4 but for earth models  $L$  (solid) and  $L'$  (dashed) and load model  $A$  with  $n = 15$ .

difference between earth models  $C$  and  $C'$  is diminished, the maximum error caused by the neglect of the IGF now being about 37 m (Fig. 4f).

Figure 5 shows the corresponding results for earth models  $L$  and  $L'$  and load model  $A$  with  $n = 15$  (Fennoscandian ice sheet). As expected, the relaxation now proceeds more slowly than for  $n = 6$ . The error due to the neglect of the IGF again has its maximum at a time after unloading close to the relaxation time of the  $M_0$  mode and, for the radial surface displacement relative to the geoid, amounts to about 16 m.

In the following, only the behaviour of the radial surface displacement will be further discussed. This strategy accounts for the diminution of the errors if displacements are referred to the geoid and thus suffices to establish *upper bounds* on the errors caused by the neglect of the IGF in interpretations of shoreline data.

### 3.2.2 Load model B

Load model B admits an adequate study of the significance of the IGF also for the *marginal* and *peripheral* regions of the load. Since, in these regions, the response is strongly affected by the elastic lithosphere, only earth models  $L$  and  $L'$  are now considered. Obviously, these models ignore effects due to the core, which introduces errors when calculating land uplift for Canada. It is shown elsewhere (Amelung 1991) that this neglect is without consequences for the *modification* of the calculated land uplift caused by the IGF.

Figures 6 and 7 show the radial surface displacement for load model  $B$  with  $R_L = 1600$  km and  $R_L = 800$  km, respectively, for several distances from the load axis. For both radii, the magnitude of the error due to the neglect of the IGF has a maximum on the load axis immediately after

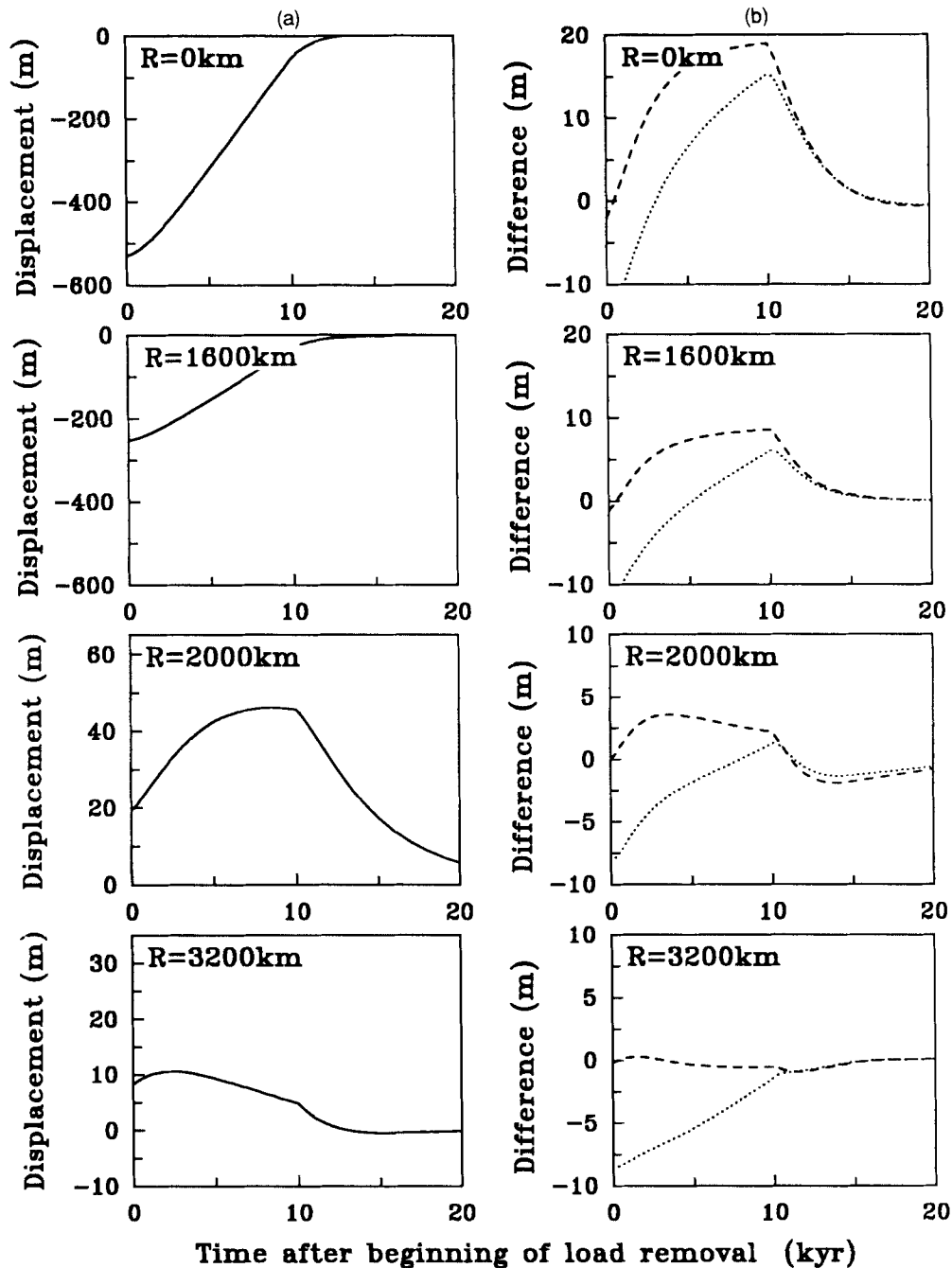


**Figure 6.** (a) Radial surface displacement,  $u_r$ , as a function of time,  $t$ , after beginning of load removal for earth model  $L$  and (b) difference between radial surface displacements for earth models  $L'$  and  $L$  (dashed) and earth models  $L''$  and  $L$  (dotted) for several distances,  $R$ , from load axis. Calculations apply to load model  $B$  with  $R_L = 1600$  km.

the end of deglaciation and reaches about 18 m and 17 m for  $R_L = 1600$  km and  $R_L = 800$  km, respectively. Thus, in comparison with instantaneous unloading, the assumption of linear unloading reduces the error considerably for a model of the Canadian ice sheet, but only slightly for a model of the Fennoscandian ice sheet. We therefore conclude that, for modelling glacial-isostatic adjustment in Canada or Fennoscandia, the IGF has similar importance although the diameters of the corresponding loads differ by a factor of two.

If, in addition to the IGF, the sphericity of the earth is neglected, we obtain the type of plane-earth model that has frequently been used in interpretations of the Fennoscandian adjustment data (e.g. McConnell 1968; Lliboutry 1971; Cathles 1975, pp. 173–196; Wolf 1987; Fjeldskaar & Cathles 1991) and, occasionally, in studies related to the Canadian data (e.g. Gasperini, Yuen & Sabadini 1990). In the following, this model will be distinguished by symbol  $L''$ .

In Figs 6(b) and 7(b), the differences between the radial surface displacements for earth models  $L''$  and  $L$  have been

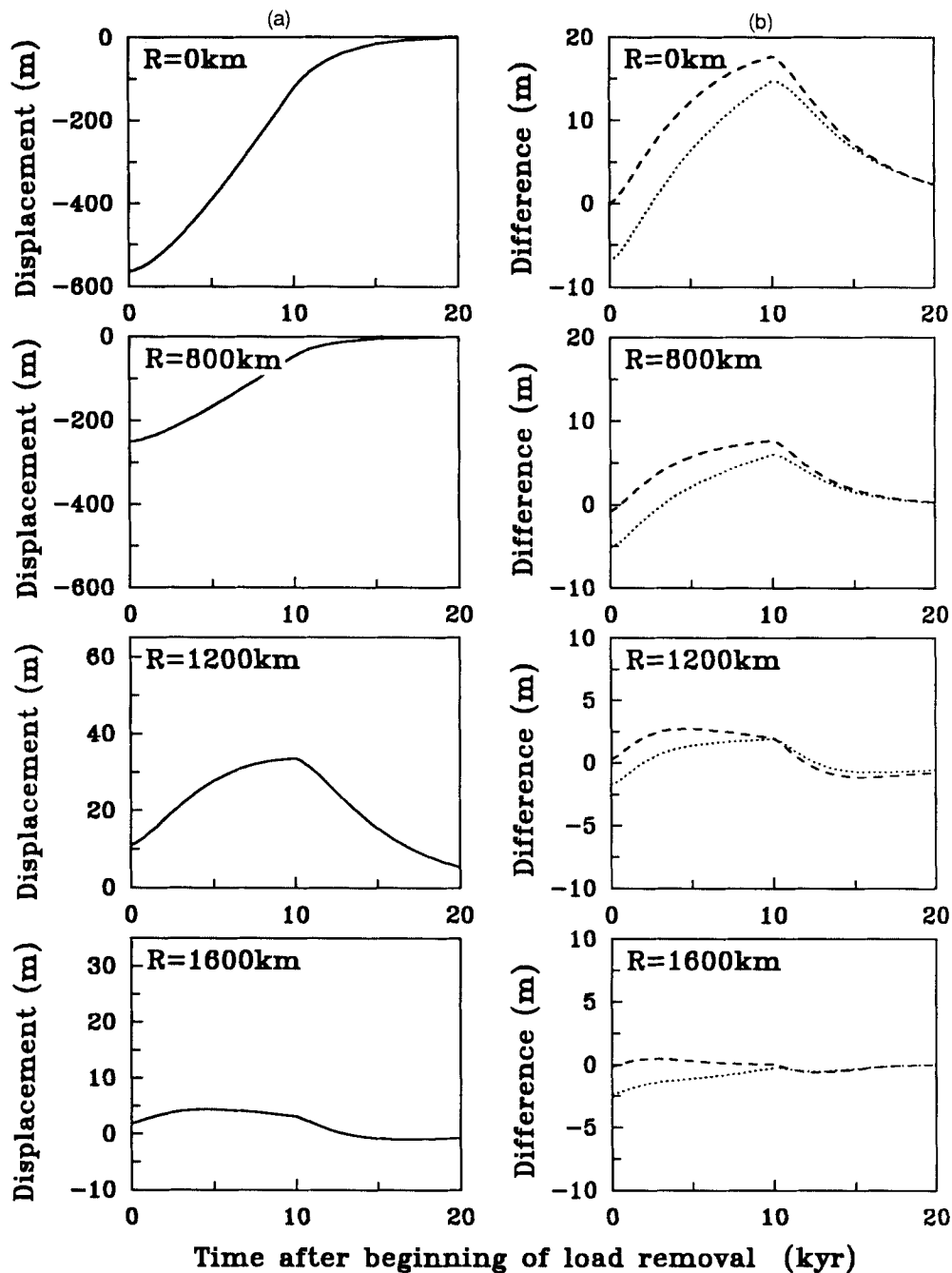


Figure 7. Same as Fig. 6 but for load model *B* with  $R_L = 800$  km.

included. Except for the beginning of deglaciation, the magnitudes of these differences are less than the magnitudes of the corresponding differences for earth models  $L'$  and  $L$ . Near the load axis, they only reach a maximum of about 15 m near the end of deglaciation for  $R_L = 1600$  km and  $R_L = 800$  km. This shows that the errors due to the neglect of the IGF and due to the neglect of sphericity partly compensate each other. The enhanced errors for earth model  $L''$  in the central regions of the loads immediately after the beginning of deglaciation are of no geophysical interest. This is because no shorelines could be formed in those regions at that time. In the marginal and peripheral

regions, the errors for earth model  $L''$  may reach almost 5 m for  $R_L = 800$  km and exceed 10 m for  $R_L = 1600$  km.

In order that the bearing of the errors entailed by earth model  $L''$  on interpretations of glacial-isostatic adjustment be assessed, we note that the errors become significant if they are comparable in magnitude to the displacements and also exceed the uncertainty of shoreline elevations. Since this uncertainty is typically about 5–10 m (e.g. Breuer & Wolf 1994), it may thus be concluded that (1) the Fennoscandian adjustment can normally be interpreted using a plane-earth model without IGF and (2) the Canadian adjustment can be interpreted with such a model

provided no high-quality data for the periphery of the load and times during deglaciation are considered. It is of interest to note that Wolf (1984) regarded the plane-earth approximation as not completely adequate for loads comparable to the Canadian ice sheet. However, Wolf based his conclusions on a simplified loading history and a comparison of the plane-earth model without IGF with the corresponding spherical-earth model without IGF and not, as has been done here, the corresponding spherical-earth model with IGF.

Finally, we note that the consideration of different field quantities or forcings may lead to different conclusions regarding the 'ranking' of earth models  $L$ ,  $L'$  and  $L''$ . An example of this is the study by Sabadini & Spada (1988), who discussed effects due to the IGF and sphericity on uplift rates for internal loading.

#### 4 CONCLUSIONS

Using *closed-form* solutions of the equations governing quasi-static gravitational-viscoelastic perturbations, induced by surface loading, of incompressible, non-rotating and initially hydrostatic fluids for two important types of spherical-earth model, we have obtained the following results.

(1) In the spherical-harmonic domain, the neglect of the IGF causes *enhancement* of the elastic amplitude of the radial surface displacement and *acceleration* of the viscous relaxation. This behaviour is a consequence of the partition of the interaction between the masses of earth, load, and surface depression into (a) the gravitational effect of the earth on the net mass of load and surface depression and (b) the net gravitational effect of load and surface depression on the mass of the earth. Since the two effects are additive, the radial surface displacement becomes larger if the second force, the IGF, is ignored.

(2) In the spatial domain, the error due to the neglect of the IGF in calculations of the radial surface displacement depends on the radius of the ice sheet and the deglaciation history adopted in the load model. For *instantaneous* deglaciation, the error is largest at a time after load removal comparable to the relaxation time of the perturbation and reaches a maximum of about 45 m (Canadian ice sheet) and about 15 m (Fennoscandian ice sheet); for more realistic *linear* deglaciation, the error is largest near the end of the deglaciation phase and reaches a maximum of less than 20 m for both load radii. These errors are further reduced by about 20 per cent if the displacements are referred to the geoid surface.

(3) Comparisons between *spherical*-earth models with or without IGF and a *plane*-earth model without IGF show that the errors resulting from the neglect of the IGF and from the neglect of sphericity partly compensate each other. As a consequence, the Fennoscandian adjustment data can normally be interpreted using a plane-earth model without IGF. This conclusion also applies to data from the centre of the Canadian ice sheet. However, high-quality data from its periphery are more accurately interpreted using a spherical-earth model with IGF.

#### ACKNOWLEDGMENTS

Constructive comments by Roberto Sabadini, Patrick Wu and an anonymous referee on an earlier draft of this paper are gratefully acknowledged.

#### REFERENCES

- Amelung, F., 1991. Viskoelastische Perturbationen sphärischer Erdmodelle: Bedeutung der Selbstgravitation beim Modellieren glazial-induzierter Relaxationsvorgänge, *Diploma thesis*, Westfälische Wilhelms-Universität, Münster.
- Breuer, D. & Wolf, D., 1992. Deglacial land emergence in Svalbard: indications of lateral inhomogeneity in the upper mantle, *Geophys. J. Int.*, submitted.
- Bullen, K.E., 1975. *The Earth's Density*, Chapman and Hall, London.
- Cathles, L.M., 1975. *The Viscosity of the Earth's Mantle*, Princeton University Press, Princeton.
- Fjeldskaar, W. & Cathles, L., 1991. Rheology of mantle and lithosphere inferred from postglacial uplift in Fennoscandia, in *Glacial Isostasy, Sea Level and Mantle Rheology*, pp. 1–19, eds Sabadini, R., Lambeck, K. & Boschi, E., Kluwer, Dordrecht.
- Gasperini, P. & Sabadini, R., 1989. Lateral heterogeneities in mantle viscosity and post-glacial rebound, *Geophys. J. Int.*, **98**, 413–428.
- Gasperini, P., Yuen, D.A. & Sabadini, R., 1990. Effects of lateral viscosity variations on postglacial rebound: implications for recent sea-level trends, *Geophys. Res. Lett.*, **17**, 5–8.
- Körnig, M. & Müller, G., 1989. Rheological models and interpretation of postglacial uplift, *Geophys. J. Int.*, **98**, 243–253.
- LePage, W.R., 1980. *Complex Variables and the Laplace Transform for Engineers*, Dover, New York.
- Lliboutry, L.A., 1971. Rheological properties of the asthenosphere from Fennoscandian data, *J. geophys. Res.*, **76**, 1433–1446.
- McConnell, R.K., 1968. Viscosity of the mantle from relaxation time spectra of isostatic adjustment, *J. geophys. Res.*, **73**, 7089–7105.
- Mitrovica, J.X. & Peltier, W.R., 1989. Pleistocene deglaciation and the global gravity field, *J. geophys. Res.*, **94**, 13 651–13 671.
- Peltier, W.R., 1976. Glacial-isostatic adjustment—II. The inverse problem, *Geophys. J. R. astr. Soc.*, **46**, 669–705.
- Sabadini, R. & Spada, G., 1988. Ground motion and stress accumulation driven by density anomalies in a viscoelastic lithosphere. Some results for the Apennines, *Geophys. J.*, **95**, 463–480.
- Smylie, D.E. & Mansinha, L., 1971. The elasticity theory of dislocations in real earth models and changes in the rotation of the earth, *Geophys. J. R. astr. Soc.*, **23**, 329–354.
- Wolf, D., 1984. The relaxation of spherical and flat Maxwell earth models and effects due to the presence of the lithosphere, *J. Geophys.*, **56**, 24–33.
- Wolf, D., 1985. An improved estimate of lithospheric thickness based on a reinterpretation of tilt data from Pleistocene Lake Algonquin, *Can. J. Earth Sci.*, **22**, 768–773.
- Wolf, D., 1987. An upper bound on lithosphere thickness from glacio-isostatic adjustment in Fennoscandia, *J. Geophys.*, **61**, 141–149.
- Wolf, D., 1991a. Viscoelastodynamics of a stratified compressible planet: incremental field equations and short- and long-time asymptotes, *Geophys. J. Int.*, **104**, 401–417.
- Wolf, D., 1991b. Boussinesq's problem of viscoelasticity, *Terra Nova*, **3**, 401–407.
- Wolf, D., 1994. Lamé's problem of gravitational viscoelasticity: the isochemical, incompressible planet, *Geophys. J. Int.*, **116**, 321–348.

- Wu, J. & Yuen, D.A., 1991. Post-glacial relaxation of a viscously stratified compressible mantle, *Geophys. J. Int.*, **104**, 331–349.
- Wu, P., 1990. Deformation of internal boundaries in a viscoelastic earth and topographic coupling between the mantle and the core, *Geophys. J. Int.*, **101**, 213–231.
- Wu, P., 1992. Deformation of an incompressible viscoelastic flat earth with power-law creep: a finite element approach, *Geophys. J. Int.*, **108**, 35–51.
- Wu, P. & Peltier, W.R., 1982. Viscous gravitational relaxation, *Geophys. J. R. astr. Soc.*, **70**, 435–486.
- Wu, P. & Peltier, W.R., 1983. Glacial isostatic adjustment and the free air gravity anomaly as a constraint on deep mantle viscosity, *Geophys. J. R. Soc.*, **74**, 377–449.

## APPENDIX A: FIELD EQUATIONS AND INTERFACE CONDITIONS: SCALAR FORMS

Assume that the centre of gravity of a fluid earth in the initial state of hydrostatic equilibrium coincides with the origin,  $O$ , of a Cartesian coordinate system,  $OX_1X_2X_3$ . Also, suppose that the fluid earth in this state has discontinuities at concentric, spherical interfaces of radii  $a_1$  and  $a_2$  about  $O$ . The symmetry of the configuration then suggests to introduce spherical-polar coordinates,  $r$ ,  $\theta$  and  $\lambda$ , by  $[X_1, X_2, X_3] = [r \sin \theta \cos \lambda, r \sin \theta \sin \lambda, r \cos \theta]$ , with  $0 < r < \infty$  the radial distance,  $0 < \theta < \pi$  the colatitude, and  $0 \leq \lambda < 2\pi$  the longitude. The two interfaces divide  $\mathcal{R}$  into three subdomains, which are uniquely determined by the following (open) intervals on the  $r$  axis:  $(0, a_1)$ ,  $(a_1, a_2)$  and  $(a_2, \infty)$ . For a point in any of the subdomains, we write  $r \in \mathcal{R}$ , where  $\mathcal{R} = (0, a_1) \cup (a_1, a_2) \cup (a_2, \infty)$ ; for a point on either of the interfaces,  $r \in \partial\mathcal{R}$  applies, where  $\partial\mathcal{R} = \{a_1, a_2\}$ . The parameters of the earth are taken as spatially homogeneous in each subdomain.

### A1 Initial state

Since  $\partial_\theta = \partial_\lambda = 0$ , the relevant spherical components of (1)–(5) are

$$\left. \begin{aligned} p_{,r}^{(0)} - \rho\phi_{,r}^{(0)} &= 0 & (16) \\ (r^2\phi_{,r}^{(0)})_{,r} &= -4\pi G\rho r^2 \end{aligned} \right\} r \in \mathcal{R}, \quad (17)$$

$$\left. \begin{aligned} [p^{(0)}]_{\pm} &= 0 & (18) \\ [\phi^{(0)}]_{\pm} &= 0 & (19) \\ [\phi_{,r}^{(0)}]_{\pm} &= 0 & (20) \end{aligned} \right\} r \in \partial\mathcal{R}.$$

### A2 Incremental state

Upon elimination of  $\tilde{r}_{ij}^{(\delta)}$ , we obtain from (6)–(13) the spherical components

$$\left. \begin{aligned} \frac{1}{r}(r^2\tilde{u}_r)_{,r} + \frac{1}{\sin\theta}(\sin\theta\tilde{u}_\theta)_{,\theta} + \frac{1}{\sin\theta}\tilde{u}_{\lambda,\lambda} &= 0 & (21) \end{aligned} \right\} r \in \mathcal{R},$$

$$\left. \begin{aligned} \nabla^2\tilde{u}_r - \frac{1}{s\tilde{m}}(\tilde{p}^{(\delta)} + \rho\gamma\tilde{u}_r - \epsilon\rho\tilde{\phi}^{(\Delta)})_{,r} \\ - \frac{2}{r^2}\tilde{u}_r - \frac{2}{r^2\sin\theta}(\sin\theta\tilde{u}_\theta)_{,\theta} - \frac{2}{r^2\sin\theta}\tilde{u}_{\lambda,\lambda} &= 0 & (22) \end{aligned} \right\} r \in \mathcal{R},$$

$$\nabla^2(\tilde{p}^{(\delta)} + \rho\gamma\tilde{u}_r - \epsilon\rho\tilde{\phi}^{(\Delta)}) = 0 \quad (23)$$

$$\nabla^2\tilde{\phi}^{(\Delta)} = 0 \quad (24)$$

$$\left. \begin{aligned} [\tilde{u}_r]_{\pm} &= 0 & (25) \\ [\tilde{u}_\theta]_{\pm} &= 0 & (26) \\ [\tilde{u}_\lambda]_{\pm} &= 0 & (27) \\ [\tilde{p}^{(\delta)} - 2s\tilde{m}\tilde{u}_{r,r}]_{\pm} &= -\gamma\tilde{\sigma} & (28) \\ [s\tilde{m}(\tilde{u}_{r,\theta} + r\tilde{u}_{\theta,r} - \tilde{u}_\theta)]_{\pm} &= 0 & (29) \\ \left[ s\tilde{m}\left(\frac{1}{\sin\theta}\tilde{u}_{r,\lambda} + r\tilde{u}_{\lambda,r} - \tilde{u}_\lambda\right) \right]_{\pm} &= 0 & (30) \\ [\tilde{\phi}^{(\Delta)}]_{\pm} &= 0 & (31) \\ [\tilde{\phi}_{,r}^{(\Delta)} - 4\pi G\rho\tilde{u}_r]_{\pm} &= -4\pi G\tilde{\sigma} & (32) \end{aligned} \right\} r \in \partial\mathcal{R},$$

where  $\nabla^2 = [\sin\theta\partial_r(r^2\partial_r) + \partial_\theta(\sin\theta\partial_\theta) + \partial_{\lambda\lambda}]/(r^2\sin\theta)$ .

## APPENDIX B: GENERAL SOLUTIONS

### B1 Initial state

We only need the general solution for  $\phi^{(0)}$ . From (16) and (17), we get

$$\phi^{(0)} = -\frac{2}{3}\pi G\rho r^2 + \frac{1}{r}D^{(1)} + D^{(2)}, \quad (33)$$

with  $D^{(1)}$  and  $D^{(2)}$  arbitrary constants. The gravity is defined by  $\gamma = -\phi_{,r}^{(0)}$ .

### B2 Incremental state

Assume that the incremental field quantities can be expanded into spherical harmonics. Since perturbations due to interface masses are studied, torsional displacements cannot be excited and only the equations for the spheroidal parts are needed. Hence, suppose solutions of the form

$$\tilde{u}_r(r, \theta, \lambda, s) = \tilde{U}(r, n, m, s)Y'_n(\theta, \lambda), \quad (34)$$

$$\tilde{u}_\theta(r, \theta, \lambda, s) = \tilde{V}(r, n, m, s)Y'_{n,\theta}(\theta, \lambda), \quad (35)$$

$$\tilde{u}_\lambda(r, \theta, \lambda, s) = \tilde{V}(r, n, m, s)\frac{1}{\sin\theta}Y'_{n,\lambda}(\theta, \lambda), \quad (36)$$

$$\tilde{p}^{(\delta)}(r, \theta, \lambda, s) = \tilde{P}^{(\delta)}(r, n, m, s)Y'_n(\theta, \lambda), \quad (37)$$

$$\tilde{\phi}^{(\Delta)}(r, \theta, \lambda, s) = \tilde{\Phi}^{(\Delta)}(r, n, m, s)Y'_n(\theta, \lambda), \quad (38)$$

where  $Y'_n(\theta, \lambda)$  are the fully normalized spherical harmonics and  $\tilde{U}(r, n, m, s)$  etc. the appropriate spherical-harmonic coefficients. Using the properties of  $Y'_n(\theta, \lambda)$ , (21)–(24) take the forms

$$\left. \begin{aligned} \tilde{U}_{,r} + \frac{2}{r}\tilde{U} - \frac{n(n+1)}{r}\tilde{V} &= 0 & (39) \end{aligned} \right\} r \in \mathcal{R},$$

$$\left. \begin{aligned} \nabla_r^2\tilde{U} - \frac{1}{s\tilde{m}}(\tilde{P}^{(\delta)} + \rho\gamma\tilde{U} - \epsilon\rho\tilde{\Phi}^{(\Delta)})_{,r} \\ - \frac{2}{r^2}\tilde{U} + \frac{2n(n+1)}{r^2}\tilde{V} &= 0 & (40) \end{aligned} \right\} r \in \mathcal{R},$$

$$\nabla_r^2(\tilde{P}^{(\delta)} + \rho\gamma\tilde{U} - \epsilon\rho\tilde{\Phi}^{(\Delta)}) = 0 \quad (41)$$

$$\nabla_r^2\tilde{\Phi}^{(\Delta)} = 0 \quad (42)$$

where  $\nabla_r^2 = \partial_{rr} + 2\partial_r/r - n(n+1)/r^2$ . Note that the

spherical-harmonic order,  $l$ , does not appear in (39)–(42), whence  $\bar{U}$ ,  $\bar{V}$ ,  $\bar{P}^{(\delta)}$  and  $\bar{\Phi}^{(\Delta)}$  depend only on the spherical-harmonic degree,  $n$ .

After elimination of  $\bar{V}$ , a system of three ordinary differential equations in  $\bar{U}$ ,  $\bar{P}^{(\delta)}$  and  $\bar{\Phi}^{(\Delta)}$  results (e.g. Wu & Peltier 1982). Introducing  $[Z_j] = [\bar{U}, \bar{V}, \bar{P}^{(\delta)}, \bar{\Phi}^{(\Delta)}]^T$ , the general solution can be written as

$$[Z_j] = \sum_{k=1}^6 A^{(k)} [Z_j^{(k)}] \left(\frac{r}{a_2}\right)^{\nu^{(k)}}, \quad (43)$$

with  $A^{(1)}, \dots, A^{(6)}$  arbitrary constants and

$$[Z_j^{(1)}] = \left[ n(n+1), n+3, 2(n+1)(2n+3) \frac{s\bar{m}}{r} - n(n+1)\rho\gamma, 0 \right]^T, \quad (44)$$

$$[Z_j^{(2)}] = [n, 1, -n\rho\gamma, 0]^T, \quad (45)$$

$$[Z_j^{(3)}] = [0, 0, \epsilon\rho, 1]^T, \quad (46)$$

$$[Z_j^{(4)}] = \left[ n(n+1), -n+2, 2n(2n-1) \frac{s\bar{m}}{r} - n(n+1)\rho\gamma, 0 \right]^T, \quad (47)$$

$$[Z_j^{(5)}] = [n+1, -1, -(n+1)\rho\gamma, 0]^T, \quad (48)$$

$$[Z_j^{(6)}] = [0, 0, \epsilon\rho, 1]^T, \quad (49)$$

$$\nu^{(1)} = n+1, \quad (50)$$

$$\nu^{(2)} = n-1, \quad (51)$$

$$\nu^{(3)} = n, \quad (52)$$

$$\nu^{(4)} = -n, \quad (53)$$

$$\nu^{(5)} = -n-2, \quad (54)$$

$$\nu^{(6)} = -n-1. \quad (55)$$

Note that  $\epsilon$  is used to distinguish the case with IGF ( $\epsilon = 1$ ) from the case without IGF ( $\epsilon = 0$ ).

## APPENDIX C: SPECIAL SOLUTIONS

### C1 Earth model L

In earth model L,  $(0, a_1)$ ,  $\bar{m}_1$  and  $\rho_1$  represent the viscoelastic mantle,  $(a_1, a_2)$ ,  $\bar{m}_2$  and  $\rho_2$  the viscoelastic lithosphere, and  $(a_2, \infty)$ ,  $\bar{m}_3 = 0$  and  $\rho_3 = 0$  the exterior of the earth. In the mantle and lithosphere, the densities are taken as identical,  $\rho_1 = \rho_2 = \rho$ .

#### C1.1 Initial state

Constants  $D^{(1)}$  and  $D^{(2)}$  in (33) are determined using (19) and (20) for  $r = a_1$  and  $r = a_2$ . Requiring also  $\lim_{r \rightarrow \infty} \phi^{(0)} = 0$ , we find

$$\phi^{(0)} = \begin{cases} -\frac{2}{3}\pi G\rho r^2 + 2\pi G\rho a_2^2, & 0 < r < a_2 \\ \frac{4}{3}\pi G\rho \frac{a_2^3}{r}, & a_2 < r < \infty \end{cases}. \quad (56)$$

The gravity at the earth's surface follows as  $\gamma_2 = 4\pi G\rho a_2/3$ .

### C1.2 Incremental state

Requiring the boundedness of the solution for  $r \rightarrow 0$  and  $r \rightarrow \infty$ , the general solution can be written as

$$[Z_j] = \sum_{k=1}^3 A^{(k)} [Z_j^{(k)}] \left(\frac{r}{a_2}\right)^{\nu^{(k)}}, \quad 0 < r < a_1, \quad (57)$$

$$[Z_j] = \sum_{k=1}^6 B^{(k)} [Z_j^{(k)}] \left(\frac{r}{a_2}\right)^{\nu^{(k)}}, \quad a_1 < r < a_2, \quad (58)$$

$$[Z_4] = C^{(6)} [Z_4^{(6)}] \left(\frac{r}{a_2}\right)^{\nu^{(6)}}, \quad a_2 < r < \infty. \quad (59)$$

The 10 constants are determined using (25)–(32) for  $r = a_1$  and  $r = a_2$ . Assuming that interface masses are present only at  $r = a_2$ , we put

$$\bar{\sigma}(a_2, \theta, s) = \bar{S}(n, m, s) Y_n'(\theta, \lambda) \quad (60)$$

and obtain with (34)–(38) the conditions

$$[\bar{U}]_{\pm}^{\pm} = 0 \quad (61)$$

$$[\bar{V}]_{\pm}^{\pm} = 0 \quad (62)$$

$$[\bar{P}^{(\delta)} - 2s\bar{m}\bar{U}_{,r}]_{\pm}^{\pm} = 0 \quad (63)$$

$$[s\bar{m}(\bar{U} + r\bar{V}_{,r} - \bar{V})]_{\pm}^{\pm} = 0 \quad (64)$$

$$[\bar{\Phi}^{(\Delta)}]_{\pm}^{\pm} = 0 \quad (65)$$

$$[\bar{\Phi}_{,r}^{(\Delta)}]_{\pm}^{\pm} = 0 \quad (66)$$

$$[\bar{P}^{(\delta)} - 2s\bar{m}\bar{U}_{,r}]_{-} = \gamma_2 \bar{S} \quad (67)$$

$$[\bar{U} + r\bar{V}_{,r} - \bar{V}]_{-} = 0 \quad (68)$$

$$[\bar{\Phi}^{(\Delta)}]_{-}^{\pm} = 0 \quad (69)$$

$$[\bar{\Phi}_{,r}^{(\Delta)}]_{-}^{\pm} + 4\pi G[\rho\bar{U}]_{-} = -4\pi G\bar{S} \quad (70)$$

Substituting for the spherical-harmonic coefficients, we finally arrive at an inhomogeneous system of 10 equations in 10 unknowns,  $A^{(1)}, A^{(2)}, A^{(3)}, B^{(1)}, \dots, B^{(6)}$  and  $C^{(6)}$ . Being interested in the solution for the interval  $(a_1, a_2)$  (lithosphere), we eliminate  $A^{(1)}, A^{(2)}, A^{(3)}$  and  $C^{(6)}$ . The residual  $(6 \times 6)$  system can be solved using standard methods. Explicit expressions for  $B^{(1)}, \dots, B^{(6)}$  are given elsewhere (Amelung 1991). Upon substitution of  $B^{(1)}, \dots, B^{(6)}$  into (58), we get in particular

$$\bar{U}(a_2) = -\frac{E_0 \bar{M}^2 + E_1 \bar{M} + E_2 \bar{S}}{F_0 \bar{M}^2 + F_1 \bar{M} + F_2 \rho}, \quad (71)$$

where  $\bar{M} = \bar{m}_1/\bar{m}_2$  and  $E_0, E_1, E_2, F_0, F_1, F_2$  are listed in Appendix E. Supposing that the mantle is *Maxwellian viscoelastic* and the lithosphere *elastic*, the corresponding relaxation functions are  $\bar{m}_1 = \mu_1/(s + \beta_1)$  and  $\bar{m}_2 = \mu_2/s$ , with  $\beta_1$  the inverse Maxwell time of the mantle and  $\mu_1$  and  $\mu_2$  the shear moduli of the mantle and lithosphere, respectively (e.g. Wolf 1991b, 1994).

### C2 Earth model C

In earth model C,  $(0, a_1)$ ,  $\bar{m}_1 = 0$  and  $\rho_1$  represent the inviscid core,  $(a_1, a_2)$ ,  $\bar{m}_2$  and  $\rho_2$  the viscoelastic mantle, and  $(a_2, \infty)$ ,  $\bar{m}_3 = 0$  and  $\rho_3 = 0$  the exterior of the earth.

## C2.1 Initial state

Constants  $D^{(1)}$  and  $D^{(2)}$  in (33) are determined using (19) and (20) for  $r = a_1$  and  $r = a_2$ . Imposing also  $\lim_{r \rightarrow \infty} \phi^{(0)} = 0$ , we get

$$\phi^{(0)} = \begin{cases} -\frac{2}{3}\pi G \rho_1 r^2 + 2\pi G [\rho_1 a_1^2 + \rho_2 (a_2^2 - a_1^2)], & 0 < r < a_1 \\ \frac{4}{3}\pi G (\rho_1 - \rho_2) \frac{a_1^3}{r} - \frac{2}{3}\pi G \rho_2 r^2 + 2\pi G \rho_2 a_2^2, & a_1 < r < a_2 \\ \frac{4}{3}\pi G [\rho_2 a_2^3 + (\rho_1 - \rho_2) a_1^3] \frac{1}{r}, & a_2 < r < \infty \end{cases} \quad (72)$$

The gravity at the CMB and at the earth's surface, respectively, follow as  $\gamma_1 = 4\pi G \rho_1 a_1 / 3$  and  $\gamma_2 = 4\pi G [\rho_2 a_2 + (\rho_1 - \rho_2) a_1^3 / a_2^2] / 3$ .

## C2.2 Incremental state

Requiring the boundedness of the solution for  $r \rightarrow 0$  and  $r \rightarrow \infty$ , the general solution reduces to

$$[Z_j] = \sum_{k=1}^3 A^{(k)} [Z_j^{(k)}] \left(\frac{r}{a_2}\right)^{\nu^{(k)}}, \quad 0 < r < a_1, \quad (73)$$

$$[Z_j] = \sum_{k=1}^6 B^{(k)} [Z_j^{(k)}] \left(\frac{r}{a_2}\right)^{\nu^{(k)}}, \quad a_1 < r < a_2, \quad (74)$$

$$[Z_4] = C^{(6)} [Z_4^{(6)}] \left(\frac{r}{a_2}\right)^{\nu^{(6)}}, \quad a_2 < r < \infty. \quad (75)$$

The 10 constants are determined using (25)–(32) for  $r = a_1$  and  $r = a_2$ . Observing that  $\bar{m}_1 = 0$  and applying interface masses at  $r = a_2$ , we get with (34)–(38) the conditions

$$[\bar{U}]_{-}^{+} = 0 \quad (76)$$

$$[\bar{P}^{(s)}]_{-}^{+} - [2s\bar{m}\bar{U}_{,r}]_{+} = 0 \quad (77)$$

$$[\bar{U} - r\bar{V}_{,r} + \bar{V}]_{+} = 0 \quad (78)$$

$$[\bar{\Phi}^{(\Delta)}]_{-}^{+} = 0 \quad (79)$$

$$[\bar{\Phi}_{,r}^{(\Delta)} - 4\pi G \rho \bar{U}]_{-}^{+} = 0 \quad (80)$$

$$[\bar{P}^{(s)} - 2s\bar{m}\bar{U}_{,r}]_{-} = \gamma_2 \bar{S} \quad (81)$$

$$[\bar{U} + r\bar{V}_{,r} - \bar{V}]_{-} = 0 \quad (82)$$

$$[\bar{\Phi}^{(\Delta)}]_{-}^{+} = 0 \quad (83)$$

$$[\bar{\Phi}_{,r}^{(\Delta)}]_{-}^{+} + 4\pi G [\rho \bar{U}]_{-} = -4\pi G \bar{S} \quad (84)$$

Note that, at the CMB,  $\bar{U}$  is taken as continuous, whereas no restriction is imposed on  $\bar{V}$ . Different displacement conditions for the CMB have been proposed in other studies (e.g. Smylie & Mansinha 1971). Substituting for the spherical-harmonic coefficients, we arrive at an inhomogeneous system of nine equations in 10 unknowns,  $A^{(1)}$ ,  $A^{(2)}$ ,  $A^{(3)}$ ,  $B^{(1)}$ ,  $\dots$ ,  $B^{(6)}$  and  $C^{(6)}$ . Being interested in the solution for the interval  $(a_1, a_2)$  (mantle), we eliminate  $A^{(1)}$ ,  $A^{(2)}$ ,  $A^{(3)}$  (which cannot be determined uniquely) and  $C^{(6)}$ , this reduces to a  $(6 \times 6)$  system for  $B^{(1)}$ ,  $\dots$ ,  $B^{(6)}$ . Explicit expressions for the constants can be found elsewhere (Amelung 1991). Upon substitution of

$B^{(1)}, \dots, B^{(6)}$  into (74), we obtain in particular

$$\bar{U}(a_2) = -\frac{E_0(s\bar{m}_2)^2 + E_1 s \bar{m}_2 + E_2 \bar{S}}{F_0(s\bar{m}_2)^2 + F_1 s \bar{m}_2 + F_2 \rho_2}, \quad (85)$$

with  $E_0, E_1, E_2, F_0, F_1, F_2$  listed in Appendix E. Supposing *Maxwellian viscoelasticity* for the mantle, we get  $\bar{m}_2 = \mu_2 / (s + \beta_2)$ , with  $\beta_2$  and  $\mu_2$  the inverse Maxwell time and the shear modulus, respectively, of the mantle (e.g. Wolf 1991b).

## APPENDIX D: IMPULSE RESPONSE

In order that the inverse Laplace transformation can be implemented, the load functions must be specified. Considering *impulsive* loading,  $S = S' \delta(t)$ , we have  $\bar{S} = S'$  and (71) and (85) can be recast into

$$\bar{U}(a_2) = -\frac{E_0' s^2 + E_1' s + E_2' S'}{s^2 + F_1' s + F_2' \rho_2} \quad (86)$$

or, alternatively,

$$\bar{U}(a_2) = -\left(T^{(c)} + T_1^{(\nu)} \frac{s_1}{s + s_1} + T_2^{(\nu)} \frac{s_2}{s + s_2}\right) \frac{S'}{\rho_2}. \quad (87)$$

We have employed

$$T^{(c)} = E_0', \quad (88)$$

$$T_1^{(\nu)} = \frac{s_1(E_1' - E_0' F_1') - E_2' + E_0' F_2'}{s_1(s_1 - s_2)}, \quad (89)$$

$$T_2^{(\nu)} = \frac{s_2(E_1' - E_0' F_1') - E_2' + E_0' F_2'}{s_2(s_2 - s_1)}, \quad (90)$$

$$s_1 = \frac{F_1'}{2} - \sqrt{\left(\frac{F_1'}{2}\right)^2 - F_2'}, \quad (91)$$

$$s_2 = \frac{F_1'}{2} + \sqrt{\left(\frac{F_1'}{2}\right)^2 - F_2'}, \quad (92)$$

$$E_0' = \frac{E_0 + E_1 M' + E_2 M'^2}{F_0 + F_1 M' + F_2 M'^2}, \quad (93)$$

$$E_1' = \frac{\beta(E_1 M' + 2E_0)}{F_0 + F_1 M' + F_2 M'^2}, \quad (94)$$

$$E_2' = \frac{\beta^2 E_0}{F_0 + F_1 M' + F_2 M'^2}, \quad (95)$$

$$F_1' = \frac{\beta(F_1 M' + 2F_0)}{F_0 + F_1 M' + F_2 M'^2}, \quad (96)$$

$$F_2' = \frac{\beta^2 F_2}{F_0 M'^2 + F_1 M' + F_2}, \quad (97)$$

with  $M' = \mu_2 / \mu_1$  (earth model *L*) or  $M' = \mu_2$  (earth model *C*),  $\beta = \beta_1$  (earth model *L*) or  $\beta = \beta_2$  (earth model *C*) and  $E_0, E_1, E_2, F_0, F_1, F_2$  from Appendix E.

The radial surface displacement in the time domain for impulsive loading follows upon inverse Laplace transformation of (87):

$$U(a_2) = -\left[T^{(c)} \delta(t) + \sum_{m=1}^2 T_m^{(\nu)} s_m e^{-s_m t}\right] \frac{S'}{\rho_2}. \quad (98)$$

**APPENDIX E: INTEGRATION CONSTANTS**

**E1 Earth model L**

In (71), we have used

$$E_0 = (2n^2 + 4n + 3) \left( \alpha^{2n} - \frac{2n+1}{2} \alpha + \frac{2n+1}{2} \alpha^{-3} - \alpha^{-2n-2} \right), \tag{99}$$

$$E_1 = -2(2n^2 + 4n + 3) \alpha^{2n} - \left[ (n^2 - 1)(2n + 3) + \frac{n(n+2)(2n^2+1)}{n^2-1} - \frac{(2n^2+4n+3)(2n+1)}{2} \right] \alpha - \frac{3(2n+1)}{2} \alpha^{-3} - \left[ 2n(n+2) + \frac{(2n^2+4n+3)(2n^2+1)}{2(n^2-1)} \right] \alpha^{-2n-2}, \tag{100}$$

$$E_2 = (2n^2 + 4n + 3) \alpha^{2n} + \left[ (n^2 - 1)(2n + 3) + \frac{n(n+2)(2n^2+1)}{n^2-1} \right] \alpha - n(n+2)(2n+1) \alpha^{-3} - \frac{n(n+2)(2n^2+1)}{n^2-1} \alpha^{-2n-2}, \tag{101}$$

$$F_0 = \frac{2n^2 + 4n + 3}{n} \frac{s\bar{m}_2}{\rho\gamma_2 a_2} \epsilon' f_0 + E_0, \tag{102}$$

$$F_1 = \frac{2n^2 + 4n + 3}{n} \frac{s\bar{m}_2}{\rho\gamma_2 a_2} \epsilon' f_1 + E_1, \tag{103}$$

$$F_2 = \frac{2n^2 + 4n + 3}{n} \frac{s\bar{m}_2}{\rho\gamma_2 a_2} \epsilon' f_2 + E_2, \tag{104}$$

$$f_0 = -\frac{n(n+2)(2n^2+1)}{n^2-1} \alpha^{2n} - \frac{n(n+2)(2n+1)^2}{2} \alpha + n(n+2)(2n-1)(2n+3) \alpha^{-1} - \frac{2n+1}{2} \left[ (n^2-1)(2n+3) + \frac{n(n+2)(2n^2+1)}{n^2-1} \right] \alpha^{-3} - (2n^2+4n+3) \alpha^{-2n-2}, \tag{105}$$

$$f_1 = \frac{2n(n+2)(2n^2+1)}{n^2-1} \alpha^{2n} + n(n+2)(2n+1) \left[ \frac{2n+1}{2} - \frac{n(n+2)(2n^2+1)}{(n^2-1)(2n^2+4n+3)} - \frac{(n^2-1)(2n+3)}{2n^2+4n+3} \right] \alpha - \frac{3n(n+2)(2n-1)(2n+3)}{2n^2+4n+3} \alpha^{-1} + \frac{3(2n+1)}{2(2n^2+4n+3)} \left[ (n^2-1)(2n+3) + \frac{n(n+2)(2n^2+1)}{n^2-1} \right] \alpha^{-3} - \left[ 2n(n+2) + \frac{(2n^2+4n+3)(2n^2+1)}{2(n^2-1)} \right] \alpha^{-2n-2}, \tag{106}$$

$$f_2 = -\frac{n(n+2)(2n^2+1)}{n^2-1} \alpha^{2n} + \frac{n(n+2)(2n+1)}{2n^2+4n+3} \left[ (n^2-1)(2n+3) + \frac{n(n+2)(2n^2+1)}{n^2-1} \right] \alpha - \frac{2n^2(n+2)^2(2n-1)(2n+3)}{2n^2+4n+3} \alpha^{-1} + \frac{n(n+2)(2n+1)}{2n^2+4n+3} \left[ (n^2-1)(2n+3) + \frac{n(n+2)(2n^2+1)}{n^2-1} \right] \alpha^{-3} - \frac{n(n+2)(2n^2+1)}{n^2-1} \alpha^{-2n-2}, \tag{107}$$

with  $\alpha = a_1/a_2$ ,  $\bar{M} = \bar{m}_1/\bar{m}_2$  and  $\epsilon' = 1$  (with IGF) or  $\epsilon' = 2(n-1)/(2n+1)$  (without IGF).

**E2 Earth model C**

In (85), we have used

$$E_0 = 0, \tag{108}$$

$$E_1 = e_1 - \epsilon G_1 e_1', \tag{109}$$

$$E_2 = G_2 (\alpha^{4n+1} - \alpha^{2n+2} - \alpha^{2n-2} + \alpha^{-1}), \tag{110}$$

$$F_0 = \frac{G_3}{3\rho_2\gamma_1 a_2} f_0, \tag{111}$$

$$F_1 = E_1 + \epsilon G_3 f_1 - 2(n-1)\epsilon' \frac{\rho_1 - \rho_2}{\rho_2} \alpha^{-2n} f_1', \tag{112}$$

$$F_2 = E_2, \tag{113}$$

$$G_1 = \frac{3(\rho_1 - \rho_2)}{2(n-1)\epsilon' \rho_2 + (2n+1)(\rho_1 - \rho_2) \alpha^3}, \tag{114}$$

$$G_2 = n\rho_2\gamma_1 a_2 \left[ \frac{3}{2(n-1)} \epsilon G_1 - \epsilon' \frac{\rho_1 - \rho_2}{\rho_2} \alpha^{-2n} \right], \tag{115}$$

$$G_3 = \frac{3\rho_1 \alpha}{2(n-1)\epsilon' \rho_2 + (2n+1)(\rho_1 - \rho_2) \alpha^3}, \tag{116}$$

$$e_1 = n(n+2) \left[ -\frac{n(n+2)(2n-1)}{n^2-1} \alpha^{-1} + (2n+1) \alpha^{-3} + \frac{2n^2+1}{n^2-1} \alpha^{-2n-2} \right], \tag{117}$$

$$e_1' = n(n+2) \left[ -\frac{2n^2+1}{n^2-1} \alpha^{2n-1} - (2n+1) + \frac{n(n+2)(2n-1)}{n^2-1} \alpha^{-2} \right], \tag{118}$$

$$f_0 = 2(n-1)(n+2) \left\{ -\frac{(2n^2+4n+3)(2n^2+1)}{n^2-1} \alpha^{2n} + (2n+1) \left[ (n^2-1)(2n+3) + \frac{n(n+2)(2n^2+1)}{n^2-1} \right] \alpha - 2n(n+2)(2n+3)(2n-1) \alpha^{-1} \right\}$$

$$+ (2n + 1) \left[ (n^2 - 1)(2n + 3) + \frac{n(n + 2)(2n^2 + 1)}{n^2 - 1} \right] \alpha^{-3} - \frac{(2n^2 + 4n + 3)(2n^2 + 1)}{n^2 - 1} \alpha^{-2n-2} \}, \quad (119)$$

$$f_1 = -\frac{n^2(n + 2)^2(2n - 1)}{n^2 - 1} (\alpha^{2n+1} - \alpha^{-2}) + (n^2 - 1)(2n + 3)(\alpha^{2n-1} - 1), \quad (120)$$

$$f'_1 = -\frac{n(n + 2)(2n^2 + 1)}{n^2 - 1} \alpha^{4n+1} - n(n + 2)(2n + 1)\alpha^{2n+2} + \left[ (n^2 - 1)(2n + 3) + \frac{n(n + 2)(2n^2 + 1)}{n^2 - 1} \right] \alpha^{2n-2} + (2n^2 + 4n + 3)\alpha^{-1}, \quad (121)$$

with  $\alpha = a_1/a_2$  and  $\epsilon' = 1$  (with IGF) or  $\epsilon' = (2n + 1)/[2(n - 1)]$  (without IGF).